Qualification Tests of 474 Photomultiplier Tubes for the Inner Detector of the Double Chooz Experiment

C. Bauer[a], E. Borger[a], R. Hofacker[a], K. Jänner[a], F. Kaether[a*], C. Langbrandtner[a],
M. Lindner[a], S. Lucht[b*], M. Reissfelder[a], S. Schönert[a], A. Stüken[b], C. Wiebusch[b]

[a]Max-Planck-Institut für Kernphysik,
Saupfercheckweg 1, D-69117 Heidelberg Germany.
E-mail: Florian.Kaether@mpi-hd.mpg.de

[b]RWTH Aachen, III. Physikalisches Institut B,
Otto-Blumenthal-Straße, D-52056 Aachen, Germany
E-mail: sebastian.lucht@physik.rwth-aachen.de

Abstract

The hemispherical 10" photomultiplier tube (PMT) R7081 from Hamamatsu Photonics K.K. (HPK) is used in various experiments in particle and astroparticle physics. We describe the test and calibration of 474 PMTs for the reactor antineutrino experiment Double Chooz. The unique test setup at Max-Planck-Institut für Kernphysik Heidelberg (MPIK) allows one to calibrate 30 PMTs simultaneously and to characterize the single photoelectron response, transit time spread, linear behaviour and saturation effects, photon detection efficiency and high voltage calibration.

Contents

*Corresponding authors

1 Introduction

Double Chooz [1] is a reactor antineutrino experiment located next to the nuclear power plant at Chooz, France. Its main physics goal is to measure a non-vanishing value of the neutrino mixing angle θ_{13} or to improve the current upper limit given by a global analysis [2]

$$\sin^2(2\theta_{13}) \leq 0.12 \text{ at } 90\% \text{ CL}. \qquad (1)$$

The two detector concept will substantially decrease systematic errors and leads to a sensitivity of

$$\sin^2(2\theta_{13}) \leq 0.03 \text{ at } 90\% \text{ CL} \qquad (2)$$

after 4 years of data taking [1]. Each of the two inner detectors of Double Chooz will be observed by 390 photomultiplier tubes (PMTs) to record light pulses produced by neutrino-induced reactions inside the gadolinium-doped scintillator target volume. The tasks of testing and calibrating these PMTs were shared between German
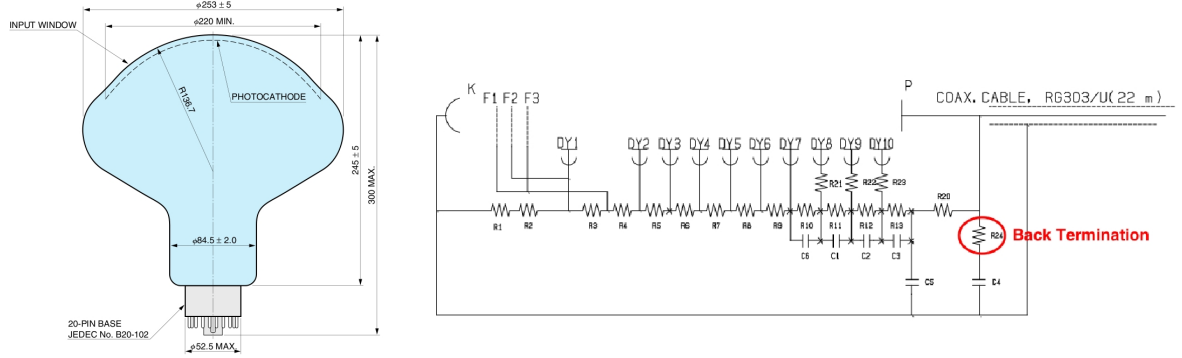
Figure 1: The PMT Hamamatsu R7081 and the base circuit used for Double Chooz (taken from [4] and [3]). R1, R2 = 2.5 MΩ; R3 = 180 kΩ; R4 = 1.02 MΩ; R5 = 1.5 MΩ; R6 = 1 MΩ; R7 = 499 kΩ; R8 = 300 kΩ; R9 = 360 kΩ; R10 = 430 kΩ; R11 = 680 kΩ; R12 = 910 kΩ; R13 = 750 kΩ; R20 = 10 kΩ; R21-R23 = 100 Ω; R24 = 49.9 Ω; C1-C3, C6 = 10nF; C4, C5 = 4.7 nF.

General parameters of R7081	Description
Spectral Response	300 to 600 nm
Peak Wavelength	420 nm
Material of photocathode	Bialkali
Effective photocathode area	220 mm dia.
Structure of dynodes	Box and Line
Number of dynodes	10
Storage Temperature	0 to +40 (°C)

Table 1: General parameters of the photomultiplier tubes Hamamatsu R7081 [4].

groups (MPIK Heidelberg and RWTH Aachen) and Japanese groups (see Acknowledgements). Both groups worked with independent calibration setups. However, careful cross-checks between both setups showed all results in good agreement. This article describes the results obtained by the German groups, and the test setup which was built at MPIK Heidelberg. The Japanese setup and results are described in [3].

The PMTs for the inner Double Chooz detector are 10 inch in diameter and have a hemispherical surface with a bialkali photocathode (type R7081MOD-ASSY) from HPK [4] (see Figure 1 and Table 1). They are made of glass which is optimized for radiopurity. The specifications of the PMTs (see Table 2) have been validated for the purpose of a preselection for the Double Chooz experiment. Furthermore, detailed characterizations of the PMT behaviour are required for a precise understanding of the final detector response.

These aims lead to the following calibration procedure which is performed for every PMT:

1. investigation of the dark count rate during and after the stabilization phase
2. determination of the high voltage (HV) value for a gain of 10^7 per photoelectron
3. characterization of the single photon electron (SPE) response regarding spectral energy resolution and peak to valley ratio
4. exploration of relative transit times and the transit time spread for single events
5. verification of the linear behaviour of the PMT signals up to high light intensities
6. determination of the photon detection efficiency (product of quantum efficiency and collection efficiency)
7. exploration of the afterpulse probability and their time characteristics
8. search for flashing PMTs

Besides the description of the test facility the following sections focus on the analysis and the results for the topics 1-6. The analysis of 7. and 8. is still ongoing and will be discussed in a separate publication.

2   Test Facility

The test facility for the above characterizations of the PMTs was built at MPIK in Heidelberg. The facility provides the possibility to measure 30 PMTs simultaneously during one calibration-run.

Parameter	Min.	Typ.	Max.	Unit
Supply voltage for gain of 1 x 10^7	1150	1500	1650	V
Anode dark count	-	4000	8000	1/s
Peak to valley ratio at SPE	2.5	2.8	-	-
Transit time spread (FWHM)	-	3.4	4.4	ns
After pulse probability (100 ns to 16 μs after main pulse)	-	-	10	%
Quantum efficiency at 420nm	22	25	-	%

Table 2: PMT characteristics (and acceptance limits) at 25°C and supply voltage for a gain of 1 x 10^7 provided by Hamamatsu.

During the whole calibration phase, three so called "reference PMTs" stayed in the setup and allowed to monitor the stability of the setup. Furthermore, the quantum efficiencies of these PMTs were absolutely calibrated by HPK which enables relative sensitivity measurements. In this section we describe the setup, in particular the different light sources used, the electronics and the data acquisition.

2.1 Setup of the Test Facility

The test facility was built inside a large 30 m^3 steel box. This, in the following called "Faraday room", is well protected against external electromagnetic fields and is closed light-tight. To prevent undesirable light reflections, the inner walls have been covered with black fire-proof rag.

Figure 2 shows the topview of the Faraday room. The PMTs are mounted in slots of a racking system which consists of six rows and five columns (see Figure 3). As denoted in Figure 2, each slot is
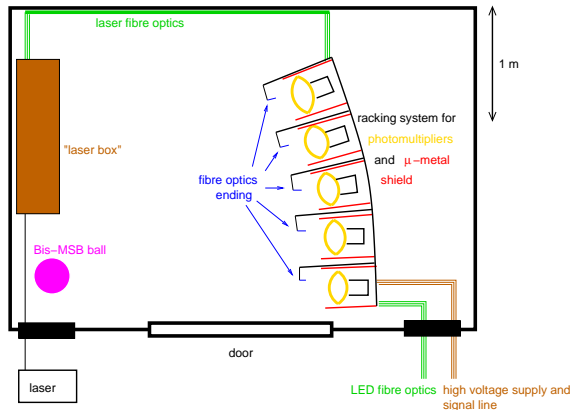
oriented towards the bis-MSB-ball, a central light source which allows one to illuminate all PMTs simultaneously. A metal arm at each slot feeds optical fibres coming from external light sources (see section 2.2) to illuminate each PMT individually. The distance between the photocathode of a PMT mounted on the rack and the fibre attachment was chosen by two criterias with respect to the solid angle of the light spread at the end of the fibre. On one hand the photocathode should be fully illuminated, on the other hand light emit-
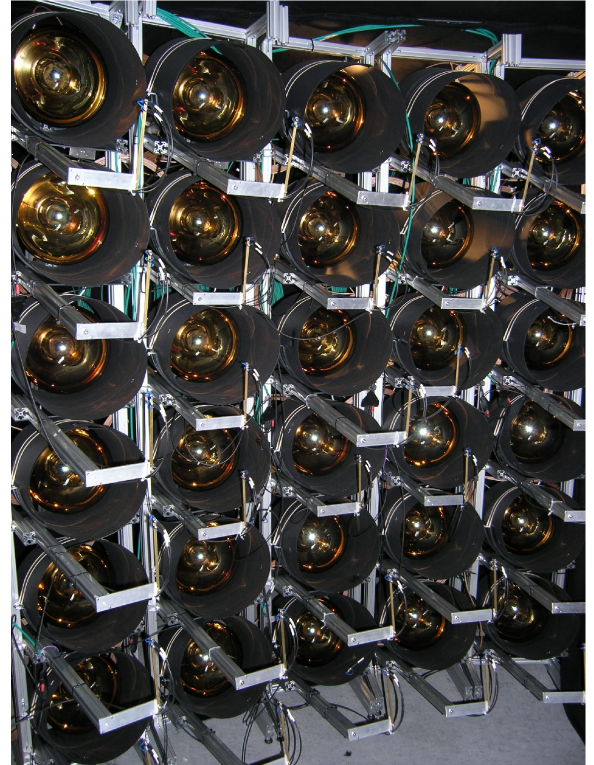

Figure 3: The PMT racking system with mounted PMTs.

Figure 2: Topview of the Faraday dark room containing the racking system for 30 PMTs.

ted from the fibre should not illuminate adjacent PMTs. Tests showed that both requirements were realized by a distance of about 50 cm between the end of the optical fibre and the photocathode.

For further magnetic shielding, a μ-metal cylinder covered by black paperboard is mounted in each slot. These cylinders have been produced for the use in the Double Chooz Experiment [5].

2.2   Light sources

Three different light sources were used.

- **LED-boards:** These VME controllable 12-channel boards were developed by the electronic workshop at MPIK. The LEDs produce light at a wavelength of 380 nm with a light intensity that can be programmed for each channel individually from the SPE range up to a few hundred PEs. The light is transmitted by optical fibres to each PMT.

- **Laser:** For measurements which require a high precision in timing we used a Picosecond Injection Laser (Advanced Laser Diode Systems A.L.S. GmbH) at a wavelength of 438 nm with a time jitter of 35 ps. Inside the light tight laser box (see Figure 2) the light pulses are widened with a diffusor lens and shines on a perforated plate where optical fibres are connected which lead to the PMT rack. Because of this configuration, small differences of the light intensity are possible for different rack slots.

- **Bis-MSB-ball:** This is a central light source of the test system. The glassblower workshop at MPIK built a quartz ball with a diameter of 11 cm which was filled with a bis-MSB/ethanol solution. Bis-MSB is a wavelength shifter which is also used for the scintillator of the Double Chooz experiment [1]. The maximal spectral emission is at a wavelength of 420 nm and matches the optimal sensitivity of the PMTs [4]. Four optical fibres are attached to guide LED signals via a quartz cylinder into the centre of the ball where the bis-MSB generates an isotropic light emission to illuminate the full PMT array.

Figure 4: The bis-MSB ball with attached optical fibres.

2.3   Electronics and Data Acquisition System (DAQ)

The front end electronics and DAQ system is located outside of the Faraday room. The PMT cables are fed through the Faraday room's wall and are connected to splitter boxes where the signals are decoupled from the supply voltage. The splitter boxes are designed and produced by the CIEMAT group (Madrid) for the Double Chooz experiment. The high voltage supply is a SY2527 Universal Multichannel Power Supply System (CAEN) [6] which provides a 500 mV resolution for voltage setting and monitoring. The modules for processing and acquiring the PMT signals are based on standard NIM modules and a VME system, respectively. Figure 5 shows a schematic illustration of the data acquisition system.

In order to exploit the full dynamic range of the used acquisition modules and to provide the required logical signals, several NIM-modules are used:

- $4\times$ sixteen channel amplifier (fixed gain $\times10$, Phillips Scientific (PS) [7] Mod. 776).

- $4\times$ octal discriminator (threshold ≥ 10 mV, PS Mod. 710).

- $4\times$ octal linear Fan-Out (PS Mod. 748).

The used acquisition modules are listed below:

- 32 channel charge-to-digital-converter (QDC V792, 12 bit resolution (400 pC), CAEN [6])
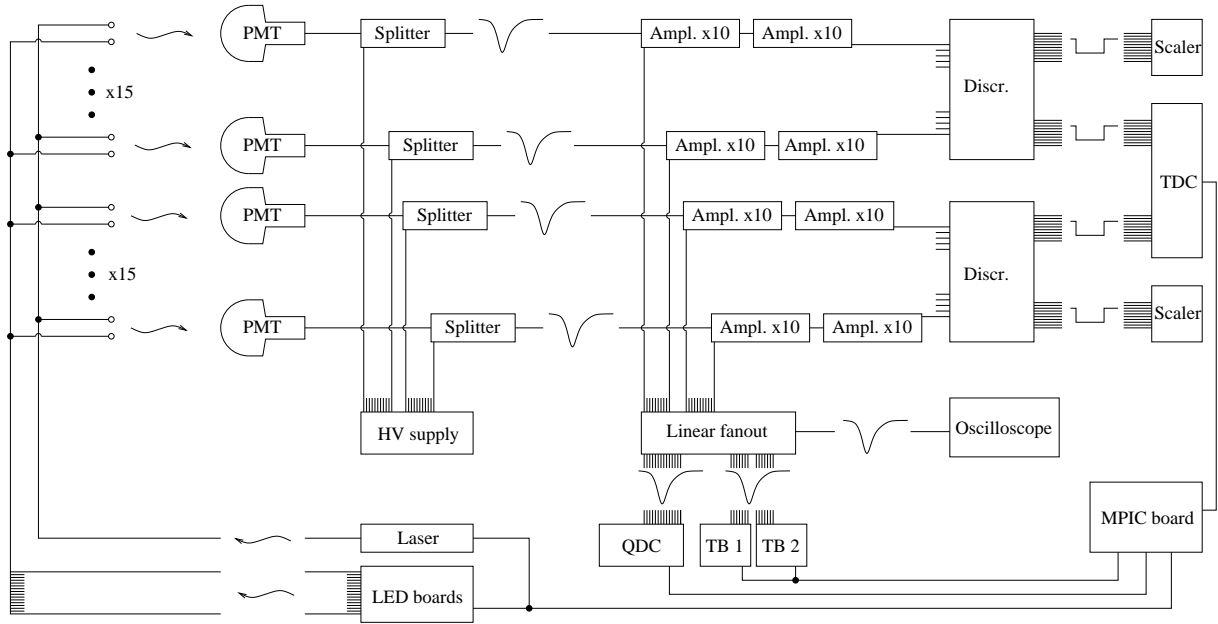
Figure 5: Schematic diagram of the electronics setup and the DAQ.

- 32 channel time-to-digital-converter (TDC V775, 12 bit resolution ($400-1200$ ns), CAEN)
- 2×16 channel Scaler (V260E, 24 bit channel depth / 100 MHz counting rate, CAEN)
- The Double Chooz Trigger Board (DC-TB), RWTH Aachen [8].

All trigger signals, gate widths etc. for the measurements were provided by the MPIC-board, which was developed at the electronic workshop at MPIK. This board provides up to 15 logic signals with free programmable gate widths and delays.

3 Measurements and results

3.1 Dark count rate behaviour

Dark count events are caused by thermal emission of electrons from the photocathode which are not distinguishable from events caused by regular photoelectrons. The major part of these events are caused by single electrons. We measured the dark count rate with a discriminator threshold at 1/4 SPE pulse amplitude height (corresponding to 1 mV for an unamplified signal at a gain of 10^7).

If PMTs are exposed to light, which is unavoidable during the installation of the PMTs at the test setup, the dark count rate is increased during the first hours after turning on the high voltage. This phase of stabilization was monitored for a period of typically 20 hours with a scaler and the DC-Trigger-Board (see Figure 6, left). After this period of time, the rate has decreased to a reasonably stable value and all calibrations which will be described in the following sections were performed. Afterwards, the dark count rate was observed again for about one day to determine the final value and to inspect its stability.

The dark count rate depends on the temperature. During the measurements the temperature inside the laboratory at MPIK was stabilized by air conditioning at $(20 \pm 1)°C$. We observed a change of the rate of roughly 100 c/s (counts/second) per $1°C$ temperature difference. Inside the Chooz underground laboratory the temperature is about $14°C$, therefore the dark count rate is expected to be lower in the final detector.

The specification for the Double Chooz experiment is a dark count rate below 8000 c/s per PMT. With one exception, all tested PMTs showed much smaller values with an average of 2200 c/s at $20°C$ with a standard deviation of 500 c/s.

To quantify the stability of the dark count rate, we calculated the root mean square (RMS) of taken data points during the stable phase (see Fig-
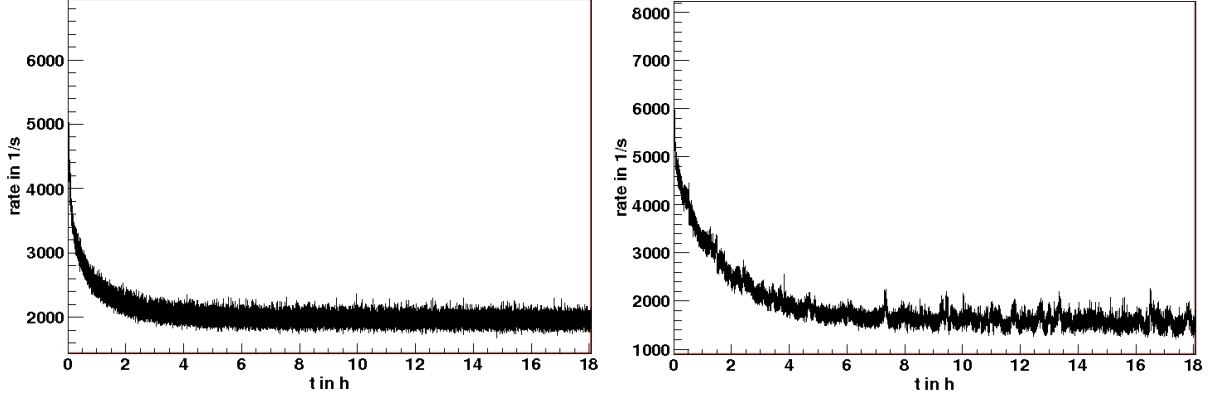
Figure 6: Left: typical dark count rate behaviour during the first hours after installation. Right: example for an unstable dark count rate.
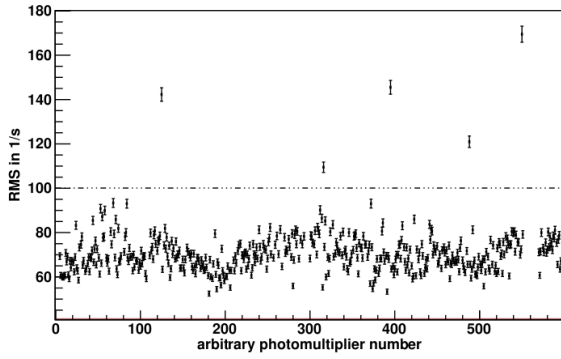

Figure 7: RMS value from the last 20 minutes in the dark count rate measurement.

ure 6, right) to compare it with the value which is expected for statistical fluctuations. If the RMS was significantly higher (see Figure 7) the PMT was not used for the Double Chooz detector.

3.2 Gain Calibration

For this measurement, we used the LEDs at SPE level. The light intesities were adjusted in such a way that on average only one out of ten triggers gives a PMT signal. Assuming that the number of created photoelectrons per event n_{PE} is poisson distributed, the probability of $n_{PE} \geq 2$ is only about 0.5%. Therefore almost pure SPE spectra were observed. The total trigger rate of LED pulses was 1 kHz. For each PMT, we took nine charge spectra (over 400 s each which cor-

responds to 400k events) at high voltage values HV_j ($j = 1, \ldots, 9$) ranging between $\pm$ 200 V around the nominal high voltage HV_{nom} (which is the value for a gain of 10^7 as provided by HPK). The signal current arriving at the QDC was integrated within a time window of 200 ns. This leads to charge spectra for which an example is shown in Figure 8. To analyse these spectra the pedestal peak was fitted by a Gaussian $Ped(i)$

$$Ped(i) = \frac{N_{Ped}}{\sqrt{2\pi}\sigma_{Ped}} \exp\left(-\frac{(i - \mu_{Ped})^2}{2\sigma_{Ped}^2}\right) . \quad (3)$$

To describe the SPE peak a combination of an exponential and a Gaussian $SPE(i)$ was used

$$SPE(i) = \frac{N_{SPE}}{\sqrt{2\pi}\sigma_{SPE}} \exp\left(-\frac{(i - \mu_{SPE})^2}{2\sigma_{SPE}^2}\right) +$$

$$+ \frac{N_{Exp}}{\tau} \exp\left(-\frac{(i - i_{min})}{\tau}\right) . \quad (4)$$

N_{Ped} and N_{SPE} are the number of entries in the pedestal and the SPE peak, respectively. μ_{Ped} and μ_{SPE} are the mean values of the fitted Gaussians, σ_{SPE} and σ_{Ped} their standard deviations, N_{Exp} and τ are the free fit parameters of the exponential which is an empirical function to describe bad amplified events, i is the number of the QDC-bin and corresponds to a charge of $i \cdot 400/4096$ pC, i_{min} is the endpoint of the pedestal fit and the starting point for the exponential fit which is roughly determined by the valley position.
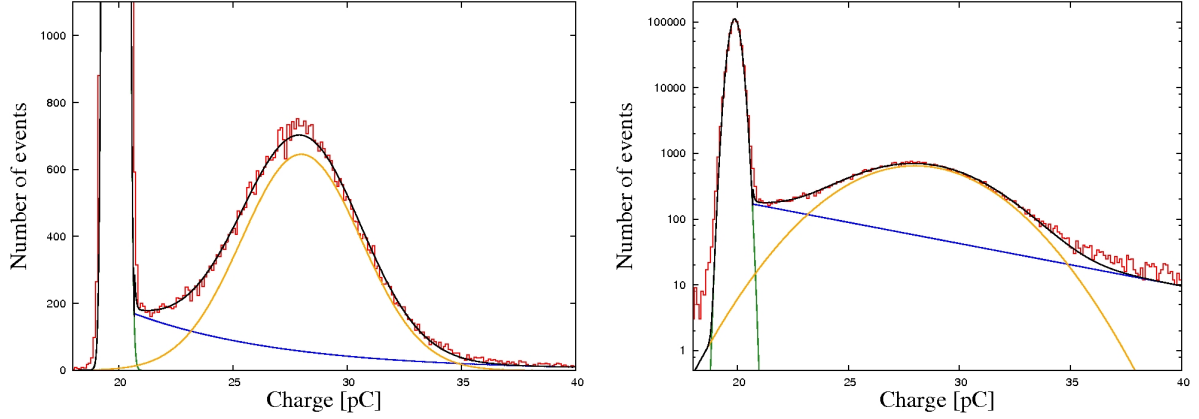
Figure 8: SPE charge spectrum in linear and logarithmic view, together with fit functions for pedestal and SPE peak. The red line shows raw QDC data. The pedestal peak was fitted by a Gaussian (green). The functions whose combination describe the SPE peak (see text) are shown in blue and orange. The black line is the combination of all fit functions which describes the complete spectrum.

The fit functions and their combination are drawn in Figure 8 showing model and data in good agreement. From the results of both fits the average charge Q corresponding to a SPE-signal is calculated

$$Q = \mu_{\text{SPE}} - \mu_{\text{Ped}}. \qquad (5)$$

For the nine different high voltage values HV_j, the corresponding charges $Q(\text{HV}_j)$ are shown in Figure 9. The $Q(\text{HV})$ dependence is fit with a power law function

$$Q(\text{HV}) = 8.0\,\text{pC} \cdot \left(\frac{\text{HV}}{\text{HV}_{\text{opt}}} \right)^{\alpha}. \qquad (6)$$

The free fit parameters are HV_{opt} and α, where HV_{opt} is the searched value for a gain of 10^7 which corresponds to an average charge of $8.0\,\text{pC}$[1]. The obtained results of HV_{opt} for all tested PMT are presented in a histogram shown in Figure 10 (left), together with the values HV_{nom} provided by HPK. The good correlation between these values is shown in Figure 10 (right).

For the verification of the obtained results and a detailed characterization of the SPE response of each PMT an additional SPE charge spectrum

Figure 9: Example of a power law fit for determination of HV_{opt}. The black points represent the charge Q which was determined at a certain high voltage value according to equation (5). The solid line is the fitted power law function equation (6).

was recorded at the previously determined HV_{opt} value. The charge value for this spectrum is determined with the above procedure and is compared to the expected value of $8.0\,\text{pC}$. The results for all PMTs are shown in Figure 11. The gain values deviate from the expected gain with a Gaussian distribution and relative RMS of 1.3%.

Finally, we investigate the stability of the three reference PMTs which are repeatedly measured in each data run at fixed positions in the rack. Figure 12 shows the determined HV_{opt} values as a func-

---

[1]A gain of 10^7 corresponds to a charge of $10^7 e = 10^7 \cdot 1.602 \cdot 10^{-19}\text{C} = 1.602\,\text{pC}$. An additional 50Ω back termination of the PMTs causes a division by a factor of 2, finally an amplification ($\times 10$) in the electronics chain leads to a value of $8.0\,\text{pC}$.
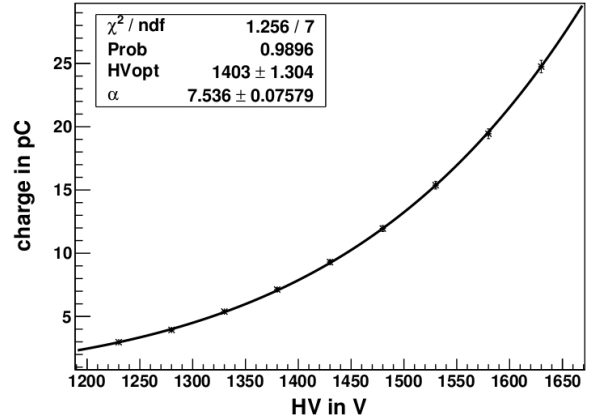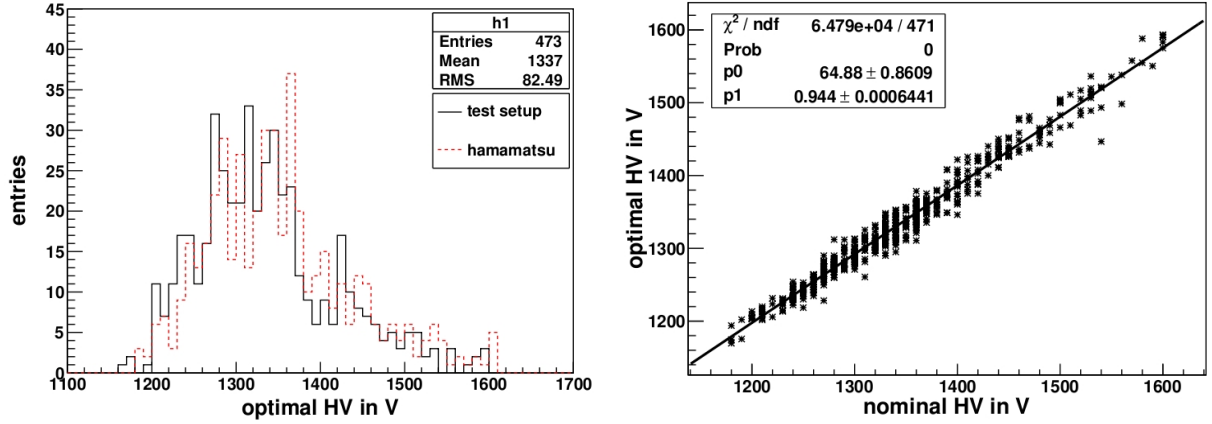
Figure 10: Left: Distribution of determined values HV_{opt} (solid line) for a gain of 10^7 compared to the values HV_{nom} provided by HPK (dotted line) of all tested PMTs. Right: HV_{opt} values versus the corresponding values HV_{nom}. Both design and actual HV values are confirmed to be consistent.
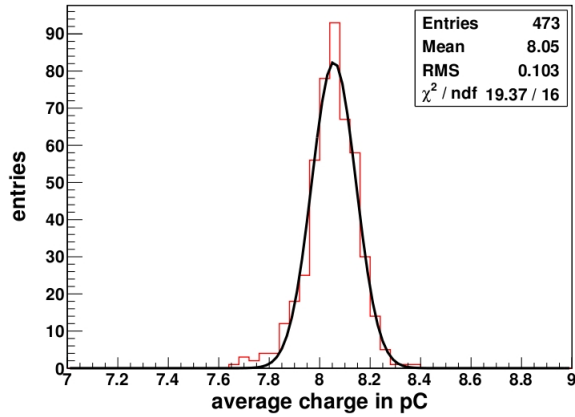

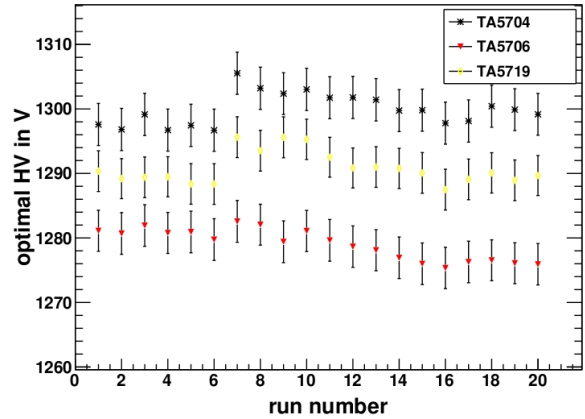**Figure 11**: Average charge value of SPE signals at HV_{opt}.

Figure 12: HV_{opt} of the reference PMTs versus the run number.

tion of the consecutive run numbers of successive PMT calibrations (corresponding to a period of about three months in total). The obtained values HV_{opt} agree within a few Volts, however a peculiar step is observable at run 7. Before this run, it was necessary to change some amplifier and fan-out channels which required re-calibrations for these channels. The visible step is consistent with an assumed systematic error of the calibrations of about 1% (which was determined using a pulse generator). In Figure 13 the determined pedestal values are shown in a histogram. The average relative spread of less than a half percent of the determined pedestal values shows a good stability of the test setup.

3.3   SPE response - charge and transit time

The PMT response for SPE pulses was characterized in detail using the high voltage HV_{opt}. The DAQ provides the possibility to record simultaneously charge and transit times for each event. A typical SPE charge spectrum is shown in Figure 8. The charge resolution of the SPE peak is typically $\Delta E \approx 2\,pC$, or to give a relative number $\Delta E/E \approx 0.25$. The peak-to-valley-ratios P/V (defined as the ratio between the maximum of the SPE peak and the minimum in the valley between the pedestal and the SPE peak) is in the range of $3.2 \leq P/V \leq 5.5$. The results for all tested PMTs are shown in Figure 14. These numbers were im-
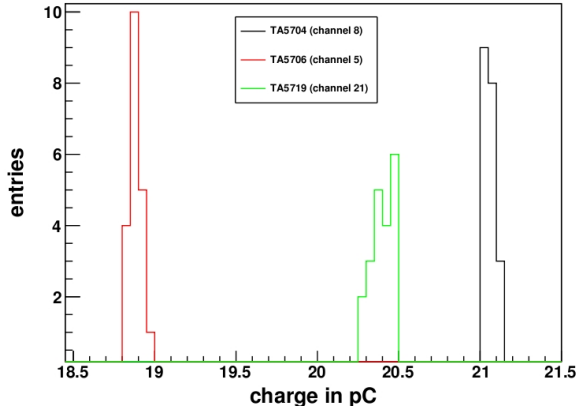
Figure 13: Histogram of the determined pedestal values of the reference PMTs.

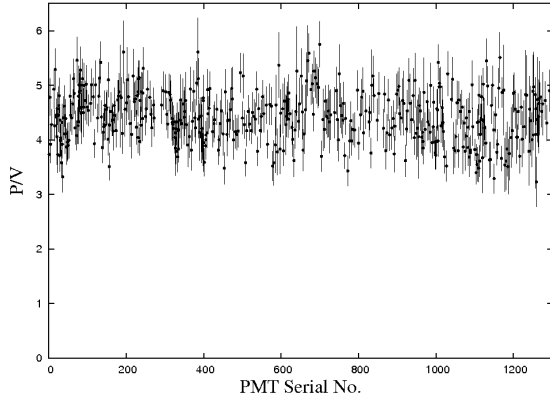**Figure 15**: Results for all tested PMTs regarding transit time spread.

Figure 14: Results for all tested PMTs regarding Peak-to-valley-ratio.

proved substantially from previous smaller values after the introduction of the μ-metal shields.

The absolute transit times were measured including an additional offset related to the electronics and the used light source. The distribution of relative transit times is shown in Figure 16 (left). Most of the events occur at roughly the same time after the time of the Laser trigger which defines $t = 0$. This main peak can be described by the sum of two Gaussians. The transit time spread is defined as the width of this peak (full width at half maximum), the results of all tested PMTs are shown in Figure 15. The average transit time spread (FWHM) is 2.8 ns with an RMS of 0.2 ns.

In addition to the main peak two more classes of events can be identified in the transit time dis-
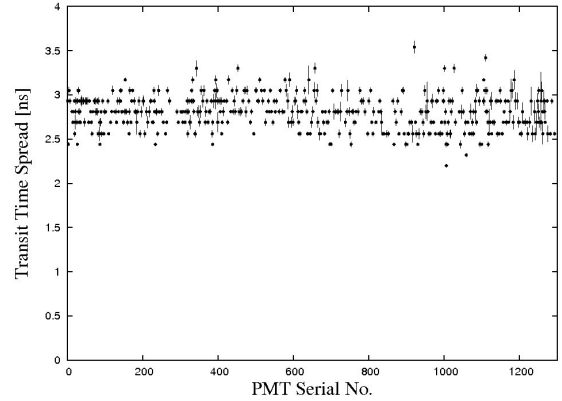
tribution: pre- and late-pulses[2]. Pre-pulses are appearing about 30 ns before the main peak. They are presumably caused by photons which pass the photocathode and hit the first dynode producing a photoelectron. In this case one step of the electron multiplication is missed, and the charge of pre-pulses is lower than the SPE value. Late-pulses appear if photoelectrons are (in)elastically scattered at the dynode, reflected and re-accelerated. These late-pulses appear up to 80 ns later than the main pulses and have a slightly smaller charge than regularly accelerated photoelectrons. The charge-transit time correlation is shown in Figure 16 (right). The probability of pre-and late-pulses are roughly 0.1% and 3%, respectively.

3.4 Verification of linear behaviour up to high light intensities

The expected light levels of neutrino events in the Double Chooz experiment are typically in the range of a few PE. Nevertheless, signals induced by cosmic muons, fast neutrons etc. may exceed the SPE region substantially. Therefore we studied the linear behaviour of the PMTs up to light intensities corresponding to 30 photoelectrons (PE) (in a few cases, up to 300 PE).

The measurement proceeds similar to the gain calibration except for the use of the bis-MSB-ball as central light source. Because of the higher

---

[2]Please note that the used single-hit TDC is not sensitve for afterpulses (caused by ionized residual gas) since only the first event after the light trigger is recorded.
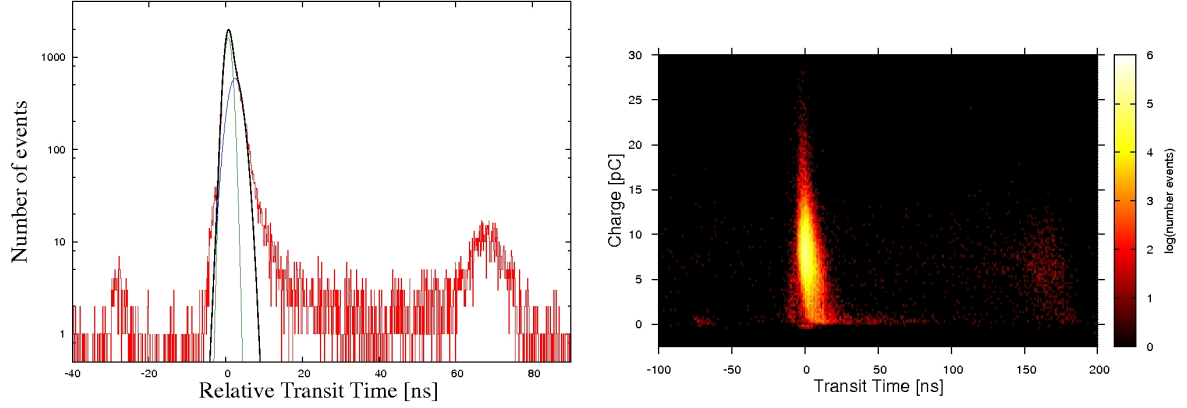
Figure 16: Left: typical distribution of relative transit times including main-, pre- and late pulses. Right: charge versus transit time plotted event by event.

light intensity almost every pulse of the bis-MSB-ball leads to PMT signals. Therefore, additional DAQ triggers without light pulses were taken for a precise pedestal determination. A typical charge spectrum is shown in Figure 17. The pedestal was fitted with a Gaussian (see equation (3)), and the spectrum was corrected for this pedestal. The charge is converted into the corresponding number of PEs, using the values determined during the gain calibration (equation (4)). The expected discrete Poissonian distribution with the mean value μ is smeard by the SPE-resolution σ. Therefore a convolution of the Poissonian with a Gaussian was used to fit the multi-PE data (MPE) and to determine μ
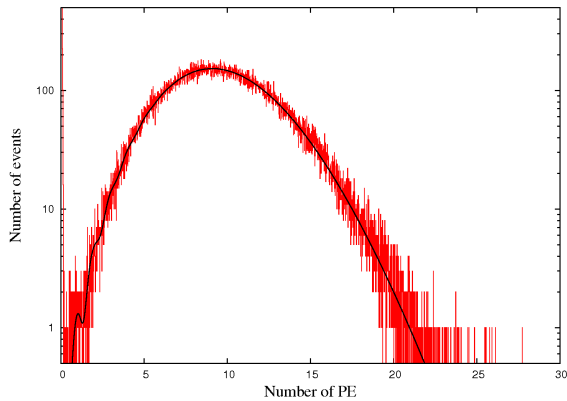

Figure 17: Typical charge spectrum for light intensities in the multi-PE region. The data (red) were fitted by the function described in equation (7) (black).

$$\text{MPE}(i) = N \sum_{k=1} \left(\frac{\mu^k}{k!} \exp(-\mu) \times \right.$$

$$\left. \times \frac{1}{\sqrt{2\pi k}\sigma} \exp\left(-\frac{(i-k)^2}{2k\sigma^2}\right) \right) . \tag{7}$$

The free fit parameter is μ which is the average number of photoelectrons. N is the total number of entries and σ the SPE resolution. i is the number of the bin of the QDC corresponding to a charge calibrated in PE.

For each PMT, nine charge spectra for the same HV_j values as for the gain calibration in section 3.2 are measured. The determined μ_j are converted to the corresponding charges Q_j which are plotted as function of the HV_j values in Figure 18. A power law function is fitted to the data and compared to the gain calibration (equation (6))

$$Q(\text{HV}) = I \cdot 8.0\,\text{pC} \cdot \left(\frac{\text{HV}}{\text{HV}_{\text{opt}}}\right)^\alpha . \tag{8}$$

The free fit parameters are the relative number of PE for this light level I and the exponent α. HV_{opt} had been determined earlier during the gain calibration (see section 3.2). In Figure 18 both HV scans are shown in double logarithmic scale. The slope α_{MPE} for higher light intensities is similar to the slope α_{SPE} at small light levels indicating a good linear response. A good linear behaviour should lead to a ratio $K = \frac{\alpha_{\text{MPE}}}{\alpha_{\text{SPE}}}$ close to unity. The resulting values of K for all tested PMTs are shown in Figure 19. The mean of the distribution
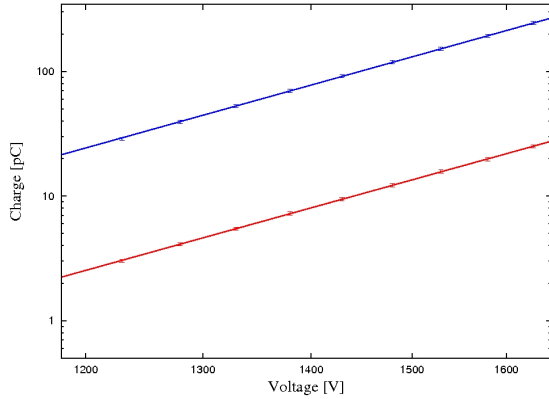
Figure 18: Average charge as a function of corresponding HV values at two different light intensities in double-logarithmic scale.

Figure 19: Distribution of the K ratios of all tested PMTs and fitted Gaussian.

is close to 1 with a spread of only 0.6%. No indications of non-linear behaviour up to signals corresponding to 30 PE were observed for any PMT.

For a few PMTs, further studies of the linear response have been performed after the completion of the calibration measurements with even higher light intensities. In order to avoid saturation of the QDC one amplifier in the DAQ chain has been removed. The results lead to the conclusion of a good linear response up to 250-300 PE when operating the PMTs at $\mathrm{HV_{opt}}$.

3.5 Determination of the photon detection efficiency

As an important characteristic of the PMTs, we determined the photon detection efficiency ε in order to identify bad PMTs. The efficiency ε is defined as the product of the quantum- and the collection efficiency $\varepsilon = QE \times CE$. The quantum efficiency (QE) indicates the ratio of the number of created PEs and the number of photons hitting the photocathode. The collection efficiency (CE) determines the number of PEs which reach the first dynode. With our setup it was not possible to measure both quantities (QE, CE) independently, however from an experimental point of view only the product ε is of interest. Following the informations given by the manufacturer, the collection efficiency is 0.9 and the quantum efficiency about 0.25 in the region of interest at a wavelength of 420 nm. The photon detection efficiency ε de-
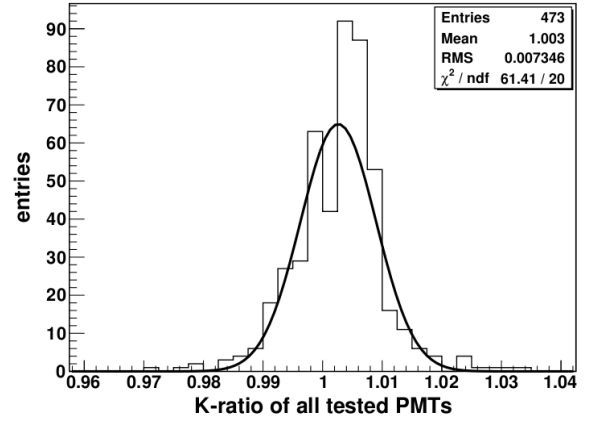
pends on the voltage between the photocathode and the first dynode, the structure of the electrical field as well as on the effective area of the first dynode.

The bis-MSB-ball is used to illuminate the complete PMT array and the absolute number of photons reaching the cathodes is unknown. Therefore, the performed calibrations are relative, comparing each PMT with the quantum efficiencies of three absolutely calibrated reference PMTs provided by HPK.

Because the light source is not perfectly stable in time, the light intensity of each event was monitored by a fixed reference PMT which remained in the same slot during all measurements. Furthermore, the geometric dependencies were calibrated by moving two additional reference PMTs subsequently slot by slot throughout the complete array. For each slot s a geometry factor g_s was determined, using the ratio of the mean values of the fixed PMT μ_{fix} and the reference PMT at the corresponding slot μ_s, defining $g_s := \mu_{\mathrm{fix}}/\mu_s$. For both reference PMTs (ref $= 1, 2$) the procedure was repeated for two different light intensities $I_{1,2}$. The final calibration for each slot was obtained by averaging

$$g_s^{\mathrm{ref}} = \frac{1}{2} \cdot \left(\frac{\mu_{\mathrm{fix}}^{I_1}}{\mu_s^{I_1}} + \frac{\mu_{\mathrm{fix}}^{I_2}}{\mu_s^{I_2}} \right). \qquad (9)$$

By comparing the response μ_{PMT} of a PMT at slot s with the simultaneous response μ_{fix} of the fixed PMT it is possible to evaluate the value $\varepsilon_{\mathrm{PMT}}$ of
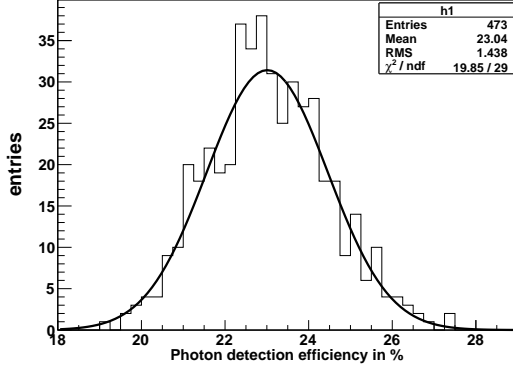
Figure 20: Photon detection efficiency $\varepsilon = CE \times QE$ of all tested PMTs and fitted Gaussian.

Figure 21: Photon detection efficiency ε versus the corresponding ScB-value.

the unknown PMT relative to the reference PMTs used during the geometric calibration

$$\varepsilon_{\mathrm{PMT}} = \frac{\mu_{\mathrm{PMT}}}{\mu_{\mathrm{fix}}} \, g_s^{\mathrm{ref}} \, \varepsilon_{\mathrm{ref}} \; . \qquad (10)$$

To increase statistics, the measurements were done at three different light intensities in the multi-PE region. In addition (as mentioned above), we used two independent reference PMTs to reduce systematic errors regarding the reference QE and in order to have a backup solution if one of the reference PMTs should show any unexpected irregularities (which did not happen). As final value we used the arithmetic mean of the six results (three intensities and two reference PMTs). For all charge spectra the same analysis methods were used as described in section 3.4.

The geometrical calibration procedure which leads to equation (9) performed at the begin and was repeated twice during the calibration phase to control the stability of the system. It turned out that the used light source (the bis-MSB-ball) was not perfectly stable with respect to geometrical anisotropies. This means the values g_s^{ref} were affected by changes in time, either slowly or stepwise which could not be determined by a backdated analysis. These shifts were probably caused by small changes of the position of the optical fibers leading light from the LED boards inside the crystal ball. Analysing the response of the two reference PMTs with respect to the fixed PMT (all these PMTs were present during the complete period of calibration) and comparing these values
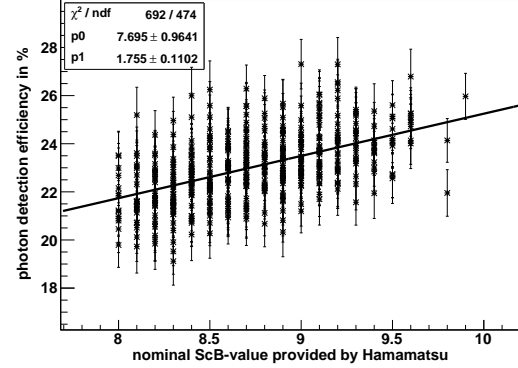
with the results of the three geometrical calibrations we estimated the relative systematical error of the photon detection efficiency to $\Delta\varepsilon \leq 5\%$. This precision is lower than expected before the calibration campaign, however it is sufficient to identify bad PMTs which was the main goal of these measurements. In total, there were only 3 PMTs with a photon detection efficiency lower than 19% which were not dedicated for installation in the Double Chooz detector.

HPK provided a value describing the sensitivity for blue light (ScB = sensitivity cathode blue index) for each PMT, which is expected to be correlated to the determined efficiency values ε. In Figure 21 the results ε of all PMTs are plotted versus their ScB-value. The correlation is obvious, although not very strong which is caused by the uncertainties of both values and differences in the collection efficiencies which are included in ε.

4   Conclusions

For the Double Chooz experiment, 474 photomultiplier tubes were tested and calibrated regarding the dark count rate, gain as a function of high voltage, SPE response, transit time spread, linear behaviour and photon detection efficiency. One PMT showed no signal at all, another one lost its vacuum after the calibration measurements for an unknown reason. For 5 PMTs we noticed an unstable dark count rate. In addition, one of them showed an inacceptable dark rate of more than

10000 c/s . For 3 PMTs we determined an photon detection efficiency lower than 0.2. In total 8 PMTs are not dedicated to be installed inside the Double detectors and will be kept as spare and to perform additional offsite tests in the future.

Acknowledgments

References

[1] F. Ardellier et al., *Double Chooz: A Search for the Neutrino Mixing Angle θ_{13}*, hep-ex/0606025v4, 2006.

[2] M. Mezzetto, T. Schwetz, *Theta_13: phenomenology, present status and prospect*, J.Phys.G37:103001, 2010.

[3] T. Matsubara et al., *Development and evaluation of 10-inch Photo-Multiplier Tubes for the Double Chooz experiment*, arXiv:1104.0786.

[4] Hamamatsu Photonics K.K., large area PMT data sheet, including R7081 (2008): http://jp.hamamatsu.com/ resources/products/etd/pdf/ LARGE_AREA_PMT_ TPMH1286E05.pdf

[5] E. Calvo et al. , *Characterization of large-area photomultipliers under low magnetic fields: Design and performance of the magnetic shielding for the Double Chooz neutrino experiment*, Nuclear Instruments and Methods in Physics Research A 621 (2010) 222-230.

[6] Data sheets at CAEN Products: http://www.caen.it

[7] Data sheets at Phillips Scientific product selection guide: http://www.phillipsscientific.com

[8] B. Reinhold, *Development and Implementation of a Level-1 Trigger and timing System for the Double Chooz Reactor Antineutrino Experiment*, phd-thesis, RWTH Aachen, 2009.